

# Dynamic performance of biomass based carbons for CO<sub>2</sub>/CH<sub>4</sub> separation. Approximation to a PSA process for biogas upgrading

**Citation for published version:**

Álvarez-Gutiérrez, N, García, S, Gil, MV, Rubiera, F & Pevida, C 2016, 'Dynamic performance of biomass based carbons for CO<sub>2</sub>/CH<sub>4</sub> separation. Approximation to a PSA process for biogas upgrading', *Energy and Fuels*, vol. 30, no. 6, pp. 5005-5015. <https://doi.org/10.1021/acs.energyfuels.6b00664>

**Digital Object Identifier (DOI):**

[10.1021/acs.energyfuels.6b00664](https://doi.org/10.1021/acs.energyfuels.6b00664)

**Link:**

[Link to publication record in Heriot-Watt Research Portal](#)

**Document Version:**

Peer reviewed version

**Published In:**

Energy and Fuels

**Publisher Rights Statement:**

This document is the Accepted Manuscript version of a Published Work that appeared in final form in Energy and Fuels, copyright © American Chemical Society after peer review and technical editing by the publisher. To access the final edited and published work see DOI: 10.1021/acs.energyfuels.6b00664

**General rights**

Copyright for the publications made accessible via Heriot-Watt Research Portal is retained by the author(s) and / or other copyright owners and it is a condition of accessing these publications that users recognise and abide by the legal requirements associated with these rights.

**Take down policy**

Heriot-Watt University has made every reasonable effort to ensure that the content in Heriot-Watt Research Portal complies with UK legislation. If you believe that the public display of this file breaches copyright please contact [open.access@hw.ac.uk](mailto:open.access@hw.ac.uk) providing details, and we will remove access to the work immediately and investigate your claim.

# Dynamic performance of biomass based carbons for CO<sub>2</sub>/CH<sub>4</sub> separation. Approximation to a PSA process for biogas upgrading.

Noelia Álvarez-Gutiérrez, Susana García<sup>†</sup>, María Victoria Gil, Fernando Rubiera, Covadonga  
Pevida\*

Instituto Nacional del Carbón, INCAR-CSIC. Apartado 73, 33080 Oviedo, Spain.

<sup>†</sup>currently at Centre for Innovation in Carbon Capture and Storage (CICCS), School of  
Engineering and Physical Sciences, Heriot-Watt University, Edinburgh EH14 4AS, United  
Kingdom

KEYWORDS. Adsorption; CO<sub>2</sub>/CH<sub>4</sub> separation; biomass based activated carbon; breakthrough  
tests.

## ABSTRACT

Physical adsorption based processes such as pressure swing adsorption (PSA) constitute  
an alternative to selectively adsorb CO<sub>2</sub> from biogas streams. There is abundant work regarding  
the equilibrium of adsorption of pure CH<sub>4</sub> and CO<sub>2</sub> on different adsorbents. However, to design

an adsorption process with a selected adsorbent it is very important to account for its dynamic behavior in a packed-bed. Thus, the performance of two biomass based activated carbons (CS-CO<sub>2</sub> and CS-H<sub>2</sub>O) previously prepared in our laboratory, to separate CO<sub>2</sub>/CH<sub>4</sub> has been evaluated. Full adsorption-desorption cycles were conducted at 30 °C (isothermal conditions) and different pressures (1, 3, 5, and 10 bar) feeding binary CO<sub>2</sub>/CH<sub>4</sub> (50/50 vol. %) mixtures to a purpose-built fixed-bed set-up. A commercial activated carbon, Calgon BPL, was also evaluated for reference purposes. CO<sub>2</sub> equilibrium uptakes were obtained from dynamic breakthrough curves and proved to be maxima at 10 bar (5.14, 4.48 and 4.14 mol kg<sup>-1</sup> for CS-CO<sub>2</sub>, CS-H<sub>2</sub>O and Calgon BPL, respectively). However the CO<sub>2</sub>/CH<sub>4</sub> separation efficiency, according to the difference in breakthrough times between CH<sub>4</sub> and CO<sub>2</sub>, is very limited at 10 bar. A combined analysis of the productivity and purity of CH<sub>4</sub> along with CO<sub>2</sub> working capacity derived from dynamic experiments indicates that our biomass based activated carbons would be better candidate materials for the CO<sub>2</sub>/CH<sub>4</sub> separation at a pressure of 5 bar than the commercial activated carbon Calgon BPL.

## INTRODUCTION

The European Union passed the Directive on Renewable Energy on December 9<sup>th</sup>, 2009 as part of the EU-Climate Change and Energy Strategy. The directive establishes an overall policy for the production and promotion of energy from renewable sources in the EU with the aim of fulfilling at least 20% of its total energy needs with renewables by 2020. It specifies national renewable energy targets for each country, taking into account its starting point and overall potential for renewables. These targets range from values as low as 10% for Malta to values as high as 49% for Sweden<sup>1</sup>. Therefore, biogas demand is expected to increase

continuously in the coming years because of its ability to produce lower CO<sub>2</sub> emissions than fossil fuels. In addition, the global capacity for power generation from commercial biogas facilities will more than double over the next decade, from 14.5 GW in 2012 to 29.5 GW in 2022<sup>2</sup>.

Since biogas contains significant amount of CO<sub>2</sub> (30-65%) <sup>3</sup> its heating value is very low compared to natural gas. Upon removal of water (vapor), hydrogen sulphide, siloxanes, hydrocarbons, ammonia and dust particles, biogas calorific value and relative density need to be adjusted in order to meet the specifications of the Wobbe Index <sup>4</sup>, i.e., biogas upgrade to natural gas quality. Towards that purpose and also to avoid pipeline and equipment corrosion, the CO<sub>2</sub> content for pipeline grade bio-methane should be less than 2-3% <sup>5</sup>. On the economical side, the removal of CO<sub>2</sub> is the most critical step in biogas upgrading. The upgrading of biogas takes between 3-6% of the energy of biogas and may cost up to 10 €/GJ for small streams <sup>6</sup>.

Currently, several methods are commercially available for the removal of carbon dioxide and other gases from biogas. These methods include adsorption <sup>7</sup>, absorption <sup>8</sup>, membranes <sup>9</sup>, and cryogenic separation <sup>10</sup>. Among these methods, pressure swing adsorption (PSA) processes have become increasingly competitive.

Biogas is usually delivered at low pressure so it needs to be compressed to a pressure between 4-10 bar before the PSA unit <sup>11</sup>. The main goal of the PSA process is to produce fuel grade methane (methane purity  $\geq 97\%$ ) <sup>12</sup>. It is however most likely that in the future more stringent specifications will apply to the methane recovery given its high Global Warming Potential <sup>13, 14</sup>. The PSA process relies on the fact that under pressure, gases tend to be attracted to solid surfaces, or “adsorbed”. The higher the pressure, the more gas is adsorbed; when the pressure is reduced, the gas is released, or desorbed. Despite the remarkable growth in practical

applications of adsorptive gas separation processes, their commercial design and optimization still require a significant experimental effort.

After original work by Sircar in the late 1980s<sup>15</sup>, many studies have been performed on PSA processes aimed at separating CO<sub>2</sub> from gaseous streams containing CH<sub>4</sub><sup>16-21</sup>. Most studies have focused on zeolites<sup>22-24</sup>, metal-organic frameworks<sup>14, 25-27</sup>, and activated carbons<sup>28-30</sup>.

Knowledge of the dynamic fixed-bed behavior is an elemental tool to validate the model used to describe the PSA performance<sup>31</sup>. Literature on the dynamic performance of adsorbent beds for CO<sub>2</sub>/CH<sub>4</sub> separation is scarce<sup>32-34</sup> and specific data on biomass based activated carbons for biogas upgrading under similar operational conditions to those presented here is lacking.

Two biomass based activated carbons (CS-CO<sub>2</sub> and CS-H<sub>2</sub>O) previously prepared in our laboratory have shown great potential for the above application based on their CO<sub>2</sub> and CH<sub>4</sub> equilibrium capture capacities (static) at high pressures<sup>35</sup>. However, as previously mentioned, the dynamic fixed-bed behavior is required to ascertain the extent to which the equilibrium uptake may be translated into breakthrough capacity. In this work, the performance of these biomass based materials has been evaluated under dynamic conditions. Hence, breakthrough experiments were performed with a simulated binary gas stream consisting of CO<sub>2</sub> and CH<sub>4</sub> (50/50 vol. %) at 30 °C and varying total pressures (1, 3, 5, and 10 bar). A commercial activated carbon, Calgon BPL, was also evaluated for comparison purposes.

Finally, the performance of the tested adsorbents over consecutive adsorption-desorption long cycles (120 to 300 min) has been used to evaluate a set of parameters for the design and optimization of a PSA process applied to biogas upgrading.

## MATERIALS AND METHODS

### Materials

Two biomass-based activated carbon samples (CS-CO<sub>2</sub> and CS-H<sub>2</sub>O) previously prepared in our laboratory from cherry stones, a low cost biomass residue from the Spanish food industry, have been evaluated as adsorbent materials. CS-CO<sub>2</sub> and CS-H<sub>2</sub>O samples were activated in a CO<sub>2</sub> and H<sub>2</sub>O single-step process, respectively. A fully detailed chemical and textural characterization of these carbons has been reported previously<sup>36</sup>. Moreover, in this study, a commercial activated carbon, Calgon BPL, was chosen for comparison purposes. Details on its chemical and textural characterization can be found elsewhere<sup>37</sup>. All gases used in this work were obtained from Air Products with purities higher than 99.995%. Table 1 summarizes the main characteristics of the evaluated adsorbents.

### Static measurements

CO<sub>2</sub> and CH<sub>4</sub> adsorption isotherms at 30 °C and up to 10 bar were determined in a high pressure magnetic suspension balance, Rubotherm-VTI. The initial mass of sample used for the adsorption isotherms was approximately 0.5 g and the equilibrium criteria was set to 0.0050 wt% change in 10 min. Prior to adsorption, the sample was dried in situ under vacuum at 100 °C for 120 min. The cell holding the sample is then cooled down to the measuring temperature, and pressurization is attained with the desired adsorbate in a stepwise mode, so the change in the weight of the adsorbent sample as well as pressure and temperature are measured and recorded when equilibrium is reached.

Experiments with helium were carried out in order to determine the volume of the adsorbent and cell system, enabling the effect of buoyancy on the measurements to be evaluated.

The absolute amount of CO<sub>2</sub> and CH<sub>4</sub> adsorbed over the pressure range tested were estimated following the procedure described in a previous work<sup>38</sup>.

#### Dynamic column breakthrough measurements

Experimental set up. All experiments were conducted in a lab-scale fixed-bed reactor packed with the adsorbent material. The main characteristics of the adsorbent beds are summarized in Table 2. It is worth pointing out that almost double amount of BPL activated carbon sample (7 g) was required for the experimental runs when compared to the biomass-based samples (4.1 g of CS-CO<sub>2</sub> and 4.8 g of CS-H<sub>2</sub>O), which was derived from targeting a similar bed height in all the experiments.

The detailed description of the system can be found elsewhere<sup>39</sup>. The stainless steel fixed-bed reactor is 13.3 cm in height, 1.3 cm in diameter and is equipped with a porous plate located 4.7 cm from the base of the column. The gas manifold system consists of three lines fitted with mass flow controllers from Bronkhorst High-Tech with flows ranging between 1 and 200 mL min<sup>-1</sup> STP. The controllers have an accuracy of 1% full scale and a repeatability of 0.1% full scale. One of the lines is used to feed in an inert gas, He, in order to dry the sample before each experiment. The other two lines feed in CO<sub>2</sub> and CH<sub>4</sub>. To monitor the column temperature a K-type thermocouple with an accuracy of ±1.5 °C was used, which is located at a height of 3.6 cm above the porous plate (exit end of the column). The mass flow rate of the effluent from the adsorbent bed was measured using a mini CORI-FLOW meter from Bronkhorst. Effluent gas analysis was performed by means of a dual channel micro-gas chromatograph, Varian CP-4900, fitted with a thermal conductivity detector (TCD) in which He and Ar were used as the carrier gases.

Breakthrough tests. Prior to each experiment, the TCD was calibrated employing CO<sub>2</sub>/CH<sub>4</sub>/He mixtures of known compositions. The bed was packed with activated carbon in order to measure the dynamics of the CO<sub>2</sub> and CH<sub>4</sub> in the column. A simulated biogas CO<sub>2</sub>/CH<sub>4</sub> mixture (50/50 vol. %) was fed (30 mL min<sup>-1</sup> STP) to the adsorption unit and the adsorption performance of the samples was evaluated at a temperature of 30 °C under isothermal conditions and four different pressures (1, 3, 5, and 10 bar). For each sample six consecutive adsorption-desorption cycles were conducted to test the reproducibility of the system, where adsorption proceeded until saturation and desorption was extended to full regeneration of the activated carbon samples.

Each experimental run involved the following steps: (i) drying of the adsorbent before each experiment by flowing He (50 mL min<sup>-1</sup> STP) for 60 min at 180 °C and atmospheric pressure, (ii) pressurization and cooling down to the adsorption temperature (30 °C) in a preconditioning step of 20 min, where 50 mL min<sup>-1</sup> (STP) of He was allowed to flow through the system, (iii) feed gas switch to a CO<sub>2</sub>/CH<sub>4</sub> gas mixture for a duration of 60 min (120-180 min for the experiments at 10 bar) so adsorption takes place until complete saturation is achieved, and (iv) depressurization of the unit and atmospheric pressure purge with 50 mL min<sup>-1</sup> (STP) of He at 180 °C for 60 min (120 min for experiment at 10 bar) to fully desorb the adsorptive gases from the column. During the adsorption stage the CO<sub>2</sub> and CH<sub>4</sub> concentrations in the column effluent gas were continuously monitored as a function of time -breakthrough curve- and maximum or equilibrium dynamic adsorption capacity of the adsorbents were calculated after the outlet CO<sub>2</sub> concentration equaled that of the inlet stream. However, in a typical operation, the flow would be stopped or diverted to a fresh adsorbent bed once the CO<sub>2</sub> concentration reached that limit<sup>40</sup>.



The equilibrium CO<sub>2</sub> adsorption capacity and breakthrough time,  $t_b$ , or time it takes for CO<sub>2</sub> to be detected at the adsorption column outlet, were calculated as an average of values obtained from six consecutive adsorption-desorption cycles. Also, as adsorbents were fully regenerated, the repeatability of breakthrough curves could be assessed. Equilibrium adsorption capacities were determined by applying a mass balance equation to the bed as well as accounting for gas accumulated in intraparticle voids and dead space of the bed<sup>37</sup>.

Blank experiments were also conducted at 30 °C and at the different pressures with a bed packed with glass beads of approximately 3 mm diameter. With these experiments extra-column effects (e.g., gas holdup) during the breakthrough tests at the different pressures could be accounted for.

## RESULTS AND DISCUSSION

### Breakthrough curves from binary CO<sub>2</sub>/CH<sub>4</sub> adsorption experiments

The CO<sub>2</sub> and CH<sub>4</sub> concentration at the outlet of the bed were measured for the adsorbents at the selected adsorption pressures and  $C/C_0$  (ratio between the outlet CO<sub>2</sub> or CH<sub>4</sub> concentration at a given time and that in the feed) was plotted versus time (Figure 1). The breakthrough times were taken at a relative concentration ( $C_{i,outlet}/C_{i,feed}$ ) of 0.05.

It is observed that after an initial period during which both components are fully adsorbed, CH<sub>4</sub> always breaks first and its breakthrough curve exhibits a so-called roll-up or roll-over, which means that the molar flow rate of CH<sub>4</sub> in the effluent is temporarily higher than that fed to the adsorption bed. The explanation for this phenomenon is that CH<sub>4</sub> is first adsorbed and thereby concentrated in the adsorbent, but then it is displaced by CO<sub>2</sub> whose concentration front advances slower through the column than that of CH<sub>4</sub>. The so-induced desorption of CH<sub>4</sub> is

responsible for a CH<sub>4</sub> flow rate rise above the feed flow rate. As time goes by, the concentration of both components at the outlet evolves to feed concentration level, indicating that the column is saturated. The preferential adsorption of CO<sub>2</sub> over CH<sub>4</sub> can be explained by the different adsorption strength of the two molecules. The permanent quadrupole moment of CO<sub>2</sub> ( $-1.4 \times 10^{-35}$  cm) leads to strong adsorption; CH<sub>4</sub>, in contrast, is not capable of similar interactions and is therefore adsorbed less strongly<sup>41</sup>. The amplitude of the roll-up is a measure of the competition between CO<sub>2</sub> and CH<sub>4</sub> for adsorption sites: it is high when a large amount of CH<sub>4</sub> is rapidly replaced by incoming CO<sub>2</sub>. An adsorbent may be selective because it intrinsically adsorbs very little CH<sub>4</sub> (early breakthrough of CH<sub>4</sub>, weak roll-up), strongly prefers CO<sub>2</sub> over CH<sub>4</sub>, in spite of a fairly strong interaction with CH<sub>4</sub> (late breakthrough of CH<sub>4</sub>, strong roll-up), or by a combination of both effects<sup>42</sup>.

As shown in Figures 1a to 1c, consecutive breakthrough curves (identified by the same color and different symbols) practically overlap showing that adsorbents were fully regenerated and samples remained stable after six consecutive adsorption-desorption cycles. Based on observed CH<sub>4</sub> and CO<sub>2</sub> concentration fronts, CO<sub>2</sub>/CH<sub>4</sub> separation might be feasible on CS-CO<sub>2</sub> and CS-H<sub>2</sub>O samples as a clear difference in breakthrough time between CO<sub>2</sub> and CH<sub>4</sub> is observed. However, the ability to separate CO<sub>2</sub>/CH<sub>4</sub> is reduced for the commercial activated carbon Calgon BPL (Figure 1c) given the closer breakthroughs of CO<sub>2</sub> and CH<sub>4</sub>. This indicates that Calgon BPL is less selective than our carbons.

It is well known that pressure affects the shape of the breakthrough curve as well as the breakthrough time. Higher adsorption pressures (i.e., higher CO<sub>2</sub> and CH<sub>4</sub> partial pressures) lead to increase adsorbed amounts and so the concentration front of each adsorptive takes more time

to reach the bed outlet. For instance, the CO<sub>2</sub> adsorption front reaches the bed outlet after approximately 9 min at 1 bar and after 25 min at 10 bar for carbon CS-CO<sub>2</sub> (see Figure 1a).

In Figure 2 the CO<sub>2</sub> and CH<sub>4</sub> breakthrough curves for the activated carbons at each pressure studied (1, 3, 5, and 10 bar) have been overlapped for comparison purposes.

The mass-transfer zone (between the break point and saturation) where most of the change in concentration occurs becomes wider with increasing pressure (see Figure 2). For the cherry stones-based carbons this is remarkable only at 10 bar but in the case of Calgon BPL the broadening of the breakthrough curves is also observed at lower pressures. The width and shape of the mass-transfer zone depend on the mass-transfer rate, the flow rate and the shape of the equilibrium adsorption isotherm. Breakthrough curves are usually *S*-shaped due to the role of internal diffusion resistance that tends to increase when the solid becomes nearly saturated. However, if pore diffusion is controlling the rate of adsorption the breakthrough curve has the opposite shape. This could be the case for CO<sub>2</sub> adsorption on Calgon BPL at 5 and 10 bar where concave downwards curves are encountered.

In the case of CH<sub>4</sub>, the breakthrough curves at the different pressures present similar slopes for the cherry stones activated carbons. It is observed that at 10 bar the height of the roll-up decreases but it becomes broader. Calgon BPL shows a different pattern in the CH<sub>4</sub> breakthrough curves: at pressures  $\geq 5$  bar the slopes and the roll-up are remarkably different.

Blank experiments with glass beads (non-adsorbent solid) are also included in Figure 2d. As expected breakthrough times are considerably reduced with respect to the adsorption experiments and no roll-up is observed. It can be seen that the sharpness of the curves drastically changes at 10 bar. This could be a result of the volume of gas accumulated in the voids of the

bed. At higher pressures the holdup of gas in the bed could be significant relative to the amount adsorbed and this gas volume must be considered in designing the adsorption cycle.

The equilibrium adsorption isotherms of CO<sub>2</sub> and CH<sub>4</sub> for the evaluated carbons are plotted in Figure 3 for discussion purposes. Detailed description and discussion of the equilibrium of adsorption of CO<sub>2</sub> and CH<sub>4</sub> on the CS-carbons has been reported elsewhere <sup>35</sup>. When adsorption is characterized by linear isotherms broad breakthrough curves are encountered. The CO<sub>2</sub> isotherm of Calgon BPL presents a more linear pattern than the CS-carbons: the CO<sub>2</sub> uptake is below that of the CS-carbons up to pressures of around 6 bar but at higher pressures Calgon BPL exceeds that of CS-H<sub>2</sub>O and eventually reaches the uptake of CS-CO<sub>2</sub> at 10 bar. CH<sub>4</sub> adsorption follows a similar pattern for the three carbons.

The width of the mass-transfer zone is related to the bed length meaning that very long beds might be required to make the transfer zone a small fraction of the bed in contrast to adsorption with favorable isotherms. A narrow mass-transfer zone is desirable to make efficient use of the adsorbent bed and to reduce the energy cost associated with its subsequent regeneration <sup>43</sup>. In fact, an ideal sorbent would have a vertical breakthrough curve, which would be representative of negligible mass-transfer resistance and minimal axial dispersion. Nevertheless, differentiation between dispersion and mass-transfer coefficients contributions to the spreading breakthrough curves is not straightforward and will require dedicated experiments and detailed modeling calculations.

The time elapsed between the CH<sub>4</sub> and the CO<sub>2</sub> breakthrough is indicative of the separation performance of the solids bed: the greater the difference in breakthrough times between both adsorbates, the higher the separation effectiveness. Moreover, it is observed in Figures 1a to 1c that there is a time interval when high purity CH<sub>4</sub> can be recovered at the bed

outlet. Cycle times in a continuous process, such as a PSA process, will be influenced by this breakthrough time difference which, in turn, would affect the amount of pure CH<sub>4</sub> that can be produced per cycle.

The values of the breakthrough time for each sample versus the total pressure have been represented in Figure 4. Little differences are encountered between the biomass based activated carbons and the commercial activated carbon Calgon BPL in the lower pressure range (< 5 bar). At 5 and 10 bar differences between samples become apparent with CS-H<sub>2</sub>O showing the longest CO<sub>2</sub> breakthrough times. In terms of CH<sub>4</sub> adsorption, Calgon BPL shows slightly higher breakthrough times at all pressures.

At 10 bar the time lag between the CH<sub>4</sub> and CO<sub>2</sub> breakthrough curves is reduced and a significant amount of CH<sub>4</sub> is co-adsorbed with CO<sub>2</sub> on samples CS-CO<sub>2</sub> and Calgon BPL limiting the separation CO<sub>2</sub>/CH<sub>4</sub>. Peter et al. studied the dynamic adsorption-desorption behavior of CO<sub>2</sub> and CH<sub>4</sub> in amino-MIL-53(Al) at different temperatures (30, 45 and 60 °C) and pressures (1, 5 and 30 bar). They also observed that at 30 bar the time lag between the breakthrough curves for both gases decreased significantly with respect to 1 and 5 bar<sup>14</sup>.

Therefore, it is inferred from our experimental results that despite the similarities in breakthrough time the samples produced from a biomass waste present potential advantage to separate CO<sub>2</sub>/CH<sub>4</sub> mixtures over the commercial activated carbon Calgon BPL.

#### Equilibrium adsorption capacity from dynamic experiments

The adsorbed amounts of CO<sub>2</sub> and CH<sub>4</sub> calculated from the breakthrough experiments are tabulated in Table 3. The amounts of CO<sub>2</sub> and CH<sub>4</sub> adsorbed at equilibrium were determined as an average of the capture performance of the adsorbents after conducting six consecutive adsorption-desorption cycles. A mass balance equation to the bed was applied to each

adsorption-desorption cycle, which considered the gas accumulated in the intraparticle voids and dead spaces of the bed. More details about the calculation procedure can be found in Gil et al.<sup>37, 39</sup>.

While adsorption capacities are usually reported in the literature on a mass basis (e.g. mol of CO<sub>2</sub> adsorbed per kg of adsorbent), the volumetric capacities (e.g. mol of CO<sub>2</sub> adsorbed per m<sup>3</sup> of adsorbent) were also calculated, since both parameters are critical in designing adsorption separation processes<sup>44</sup>.

The uptakes obtained from the breakthrough experiments indicate that, as expected, the adsorption capacity of the activated carbons increased with pressure. For instance, the capacity values obtained at 30 °C for the CS-CO<sub>2</sub> sample rose from 1.63 to 5.14 mol kg<sup>-1</sup> adsorbent as the pressure increased from 1 to 10 bar.

The CO<sub>2</sub> adsorption capacity on a mass basis followed the order: CS-CO<sub>2</sub> > CS-H<sub>2</sub>O > Calgon BPL (Table 3). The greatest CO<sub>2</sub> adsorption capacity (5.14 mol kg<sup>-1</sup>) corresponds to the biomass based activated carbon CS-CO<sub>2</sub> at 10 bar. The CH<sub>4</sub> adsorption capacity on a mass basis showed similar trend although the difference among the uptakes of the adsorbents is less noticeable than in the case of the CO<sub>2</sub> adsorption capacity. The greatest CH<sub>4</sub> uptake on a mass basis (1.55 mol kg<sup>-1</sup>) corresponds to CS-CO<sub>2</sub> at 10 bar.

It has been previously reported that at high pressure, the total micropore volume, determined by N<sub>2</sub> adsorption isotherms at -196 °C, is the textural parameter more directly related to the CO<sub>2</sub> adsorption capacity of the materials<sup>45, 46</sup>. In fact, Wiersum et al. observed that at high pressure the solid with the largest pore volume also exhibited the highest uptakes while the solid with the smallest pore volume adsorbed the least<sup>47</sup>. However, in this work we encounter the opposite trend. Based on textural properties of the materials (Table 1), Calgon BPL is the sample

with largest micropore volume ( $0.46 \text{ cm}^3 \text{ g}^{-1}$ ) compared to CS-CO<sub>2</sub> ( $0.40 \text{ cm}^3 \text{ g}^{-1}$ ) and CS-H<sub>2</sub>O ( $0.38 \text{ cm}^3 \text{ g}^{-1}$ ). This may be attributed to the significantly narrower average micropore width of the biomass based carbons (Table 1) that also plays a significant role in high pressure adsorption<sup>46</sup>.

Comparing the calculated capacities on a volumetric basis the previous trend is reversed. The CO<sub>2</sub> adsorption capacity follows the order: Calgon BPL > CS-H<sub>2</sub>O > CS-CO<sub>2</sub> (Table 3). This is mainly attributed to a different bed weight for breakthrough tests with Calgon BPL (see bed density in Table 2) as a constant bed height was targeted for the experiments with three different adsorbents. This is a disadvantage of the biomass based carbons that could be overcome with tailored conformation during the production process. It should be noted however, that the large CO<sub>2</sub> adsorption capacity on a volumetric basis of Calgon BPL, is also accompanied by significant CH<sub>4</sub> adsorption that may lead to reduce adsorption selectivity.

#### Optimization of adsorption conditions

Generally, in a PSA process one of the feed components is preferably adsorbed in the bed (in this case CO<sub>2</sub>), while the rest of them are weakly adsorbed and leave the bed forming the raffinate. During subsequent regeneration, the CO<sub>2</sub> retained is desorbed and it is recovered as extract. Therefore, the target is to recover most, in this case CO<sub>2</sub>, as part of the extract and with the highest possible purity. Nevertheless, in biogas upgrading both raffinate (CH<sub>4</sub>) and extract (CO<sub>2</sub>) are valuable products that might be recovered at high purity. Therefore, the purity level of the CH<sub>4</sub> will be dictated primarily by the breakthrough of CO<sub>2</sub> that is first eluted from the adsorbent bed.

The dynamic experiments were conducted until saturation and complete regeneration of the solids bed were reached in each cycle. In a real PSA process the feed step is normally

terminated before the most strongly adsorbed component breaks through the bed (saturation), while the regeneration step is generally terminated before the bed is fully regenerated.

The analysis of transient breakthroughs has proved useful to evaluate the separation performance of adsorbents<sup>48</sup>. By analyzing the performance of these long cycles we can identify conditions that would be feasible in short cyclic experiments to be applied to a real PSA process aimed for biogas upgrading.

Therefore, in this work, three different parameters have been selected to account for the process performance. These are: CO<sub>2</sub> working capacity, CH<sub>4</sub> productivity and CH<sub>4</sub> purity. The last one is defined through the operating conditions of the process. As we have mentioned in the Introduction, the present study does not intend to conduct a detailed design and/or optimization of a PSA unit.

The working capacity is defined herein as the difference between the loading of the component that needs to be preferentially adsorbed, expressed in moles per kilogram of adsorbent, at the “adsorption” pressure and the corresponding loading at the “desorption”, or purge, pressure, here assumed to be 1 bar. The higher the working capacity is, the larger the amount of feed that can be treated with a given amount of adsorbent within a given period of time<sup>3, 49, 50</sup>.

The amount produced per kg of material or productivity is relevant for grass-roots design of PSA units; this metric is directly a reflection of the adsorbent cost<sup>51</sup>.

Maximum values of CO<sub>2</sub> working capacity and productivity are desired as a smaller adsorbent bed volume would be then required. Therefore, capital and operating costs would decrease.



In order to determine the pressure level for the adsorption stage, one should keep in mind that the larger the difference between the capacities of the competing adsorbates, the purer the raffinate will be. For a given separation, the product purity is predetermined and the size of the adsorbent bed is inversely proportional to the adsorbent productivity. It is important to keep in mind that these parameters are interrelated for any given PSA process<sup>17</sup>.

Design parameters. Discussion and implication for biogas upgrading. As we previously mentioned, one of the parameters that we have taken into account to compare our materials is the working capacity. The experimental working capacity of CO<sub>2</sub> was obtained by calculating the difference between the adsorbed amounts of CO<sub>2</sub> under adsorption and desorption conditions (here assumed to be 1 bar). The calculated values assuming adsorption pressures of 3, 5 and 10 bar are represented in Figure 5. As might be expected working capacity increases with pressure and the highest values for the three adsorbents are obtained at 10 bar. This is in agreement with the equilibrium adsorption capacities from static single component adsorption isotherms (Figure 3) and dynamic binary breakthrough tests (Table 3). At 10 bar it was observed previously that the efficiency of the CO<sub>2</sub>/CH<sub>4</sub> separation decreases and a great amount of CH<sub>4</sub> is also co-adsorbed with CO<sub>2</sub>. Thus, this may not be the pressure that best suits the adsorption step in this process and it will be discarded in following analysis. On the other hand, it is observed in Figure 5 that the working capacity of Calgon BPL is lower than that of CS-CO<sub>2</sub> and CS-H<sub>2</sub>O.

From the data presented in Figures 1a to 1c we can determine the amount of CH<sub>4</sub> in the exit gas stream. As illustration, Figure 6 shows the experimental breakthrough for CO<sub>2</sub>/CH<sub>4</sub> mixture (50/50 vol. %) at 30 °C and at 5 bar in the fixed bed packed with CS-CO<sub>2</sub>. The y-axis represents the % CH<sub>4</sub> in the exit gas stream. During the time interval between t<sub>1</sub> and t<sub>2</sub>, CH<sub>4</sub> can be produced with a purity of approximately 95%. Thus the productivity of CH<sub>4</sub>, with the selected

95% purity level, can be estimated from a material balance by integrating the CH<sub>4</sub> molar flow rate profile in the outlet gas between the time interval t<sub>1</sub> to t<sub>2</sub>, as follows:

$$CH_4 \text{ productivity} = \frac{1}{m_{ads} t} \int_{t_1}^{t_2} F_{CH_4, exit} dt \quad (1)$$

where F<sub>CH<sub>4</sub>,exit</sub> is the molar flow rate of CH<sub>4</sub> that exits the bed, m<sub>ads</sub> is the mass of adsorbent packed in the bed and t is the time interval (t<sub>2</sub>-t<sub>1</sub>) when CH<sub>4</sub> leaves the bed at the selected purity (~95%). Productivity, as estimated from Equation 1, is then reported in mol per kg of adsorbent and unit of time.

Figure 7 shows the amount of CH<sub>4</sub> produced in the outlet stream, per kilogram of adsorbent material and minute, versus pressure. There is not a direct correlation between the productivity of CH<sub>4</sub> and total pressure. However, it seems clear that Calgon BPL has significantly lower productivities than our adsorbents. Maximum CH<sub>4</sub> productivity of 0.26 mol kg<sup>-1</sup> min<sup>-1</sup> is achieved for CS-CO<sub>2</sub> and CS-H<sub>2</sub>O at 3 and 5 bar, respectively.

In Figure 8 the purity of CH<sub>4</sub> in the outlet gas stream is presented as a function of the total pressure in the breakthrough experiments for the three adsorbents. The concentration of CH<sub>4</sub> tends to decrease with increasing pressure and more remarkably for Calgon BPL, where the concentration of CH<sub>4</sub> is below 85% at 5 bar. However, the purity of CH<sub>4</sub> in the outlet stream remains practically constant (~ 95%) for carbon CS-H<sub>2</sub>O in the evaluated pressure range.

As mentioned above, maximum values of CO<sub>2</sub> working capacity and CH<sub>4</sub> productivity must be sought since they are closely related to the size of the adsorber. Figure 9 shows CH<sub>4</sub> productivity versus CO<sub>2</sub> working capacity for the studied carbons. As can be observed, CH<sub>4</sub> productivity slightly varies with CO<sub>2</sub> working capacity for each carbon. Thus, maximum CO<sub>2</sub> working capacity turns to be the prevailing criteria. For CS-CO<sub>2</sub>, and CS-H<sub>2</sub>O this condition is achieved at the maximum pressure of 5 bar at which CO<sub>2</sub>/CH<sub>4</sub> separation is still feasible. On the

other hand, Calgon BPL shows poor performance in terms of CH<sub>4</sub> productivity and CO<sub>2</sub> working capacity when compared to our biomass based carbons.

The experimental results show that at a pressure of 5 bar the performance of CS-H<sub>2</sub>O is slightly superior to that of CS-CO<sub>2</sub>. Despite the similar adsorption capacities on a mass basis of both CS-carbons, CS-H<sub>2</sub>O shows slightly better breakthrough time, CO<sub>2</sub> working capacity and CH<sub>4</sub> productivity and purity. Moreover, it shows enhanced adsorption capacity on a volumetric basis which would allow reduced size of the required equipment.

In a previous work<sup>35</sup> we focused on the analysis of the equilibrium of adsorption of CO<sub>2</sub> and CH<sub>4</sub> from static gravimetric isotherms up to pressures of 10 bar. Despite the great similarities of both CS-carbons in terms of adsorption capacities we identified CS-CO<sub>2</sub> as preferred adsorbent for the separation of CO<sub>2</sub> from a CO<sub>2</sub>/CH<sub>4</sub> mixture representative of a biogas stream. That conclusion was based on the enhanced values of an adsorption performance indicator that accounts for the selectivity, the working capacity and the isosteric heat of adsorption of CO<sub>2</sub>. Herein, breakthrough tests were conducted under isothermal operation and so heat effects on the adsorption performance of the adsorbents are deliberately avoided. Therefore, comparison is not straightforward. However, in the aforementioned work it was also clearly concluded that in terms of the selection parameter  $S$  (that accounts for the ratio of the working capacities of the two gases and the equilibrium selectivity to CO<sub>2</sub>), CS-H<sub>2</sub>O was slightly superior to CS-CO<sub>2</sub>. This is in good agreement with the isothermal breakthrough experiments carried out in this work that also indicate that CS-H<sub>2</sub>O presents better performance for biogas upgrading at a pressure of 5 bar.

## CONCLUSIONS

Analysis of CO<sub>2</sub> and CH<sub>4</sub> co-adsorption on two biomass based activated carbon (CS-CO<sub>2</sub> and CS-H<sub>2</sub>O) materials has been performed by means of dynamic breakthrough experiments in a packed-bed. A commercial activated carbon Calgon BPL was also studied for comparison purposes.

The evaluated adsorbents showed good cyclability and regenerability over consecutive adsorption-desorption cycles. CO<sub>2</sub>/CH<sub>4</sub> separation is feasible on CS-CO<sub>2</sub> and CS-H<sub>2</sub>O according to the difference in breakthrough time between CO<sub>2</sub> and CH<sub>4</sub>. However, this ability is reduced for Calgon BPL indicating that it is less selective than our carbons.

The adsorption pressure in a PSA process should be carefully chosen considering the process performance. We have analyzed the purity and productivity of CH<sub>4</sub> and the CO<sub>2</sub> working capacity from binary CO<sub>2</sub>/CH<sub>4</sub> equimolar breakthrough tests conducted at 30°C and varying pressures. When adsorption pressure increases CO<sub>2</sub> working capacities also increase. It is observed that when adsorption pressure increases so does CO<sub>2</sub> working capacity. However, at 10 bar the efficiency of the CO<sub>2</sub>/CH<sub>4</sub> separation drastically decreases for the evaluated adsorbents.

CS-CO<sub>2</sub> and CS-H<sub>2</sub>O have good adsorption capacities with measured CO<sub>2</sub> working capacities of 1.96 and 2.04 mol kg<sup>-1</sup> for CS-CO<sub>2</sub> and CS-H<sub>2</sub>O, respectively, when adsorbents are cycled between 5 bar of adsorption pressure and 1 bar of regeneration pressure. Maximum CH<sub>4</sub> productivities of 0.26 mol kg<sup>-1</sup> min<sup>-1</sup> are achieved for CS-CO<sub>2</sub> and CS-H<sub>2</sub>O at 3 and 5 bar, respectively. These values are higher than those of Calgon BPL (working capacity of CO<sub>2</sub> in the same conditions of 1.53 mol kg<sup>-1</sup> and CH<sub>4</sub> productivity of 0.15 mol kg<sup>-1</sup> min<sup>-1</sup> at 3 bar). On the other hand, the purity of CH<sub>4</sub> in the outlet stream for both biomass based activated carbons is above 95%. whereas for Calgon BPL the purity of CH<sub>4</sub> drastically decreases with pressure.

These values are higher than those of the commercial Calgon BPL. From the results presented it can be concluded that our biomass based activated carbons, CS-CO<sub>2</sub> and CS-H<sub>2</sub>O, are promising adsorbents for CO<sub>2</sub>/CH<sub>4</sub> separation operating at a pressure of 5 bar.

## AUTHOR INFORMATION

### Corresponding Author

\*(C.P) Phone: +34 985 11 89 87 / 985 11 90 90 (Ext. 319). Fax: +34 985 29 76 62. Email: [cpevida@incar.csic.es](mailto:cpevida@incar.csic.es).

### Author Contributions

The manuscript was written through contributions of all authors. All authors have given approval to the final version of the manuscript.

### Funding Sources

Project: ENE2011-23467 (Spanish MINECO) and GRUPIN14-079 Grant (Gobierno del Principado de Asturias, Spain).

## ACKNOWLEDGMENT

This work has received financial support from the Spanish MINECO (Project ENE2011-23467), co-financed by the European Regional Development Fund (ERDF), and from the Gobierno del Principado de Asturias (PCTI2013-2017, GRUPIN14-079). N.A-G. also acknowledges a fellowship awarded by the Spanish MINECO (FPI program), and co-financed by the European Social Fund.

- 447 1. Commision, E., Directive 2009/28/EC of the European Parliament and of the Council of  
448 23 April 2009 on the promotion of the use of energy from renewable sources and amending and  
449 subsequently repealing Directives 2001/77/EC and 2003/30/EC. In Official Journal of the  
450 European Union: 2009.
- 451 2. Research, P. Worldwide power generation capacity from biogas will double by 2022. .  
452 [http://www.businesswire.com/news/home/20121107005284/en/Worldwide-Power-Generation-](http://www.businesswire.com/news/home/20121107005284/en/Worldwide-Power-Generation-Capacity-Biogas-Double-2022%20-.U3NpFViSwwk)  
453 [Capacity-Biogas-Double-2022%20-.U3NpFViSwwk](http://www.businesswire.com/news/home/20121107005284/en/Worldwide-Power-Generation-Capacity-Biogas-Double-2022%20-.U3NpFViSwwk)
- 454 3. Remy, T.; Gobechiya, E.; Danaci, D.; Peter, S. A.; Xiao, P.; Van Tendeloo, L.; Couck, S.;  
455 Shang, J.; Kirschhock, C. E. A.; Singh, R. K.; Martens, J. A.; Baron, G. V.; Webley, P. A.;  
456 Denayer, J. F. M., Biogas upgrading through kinetic separation of carbon dioxide and methane  
457 over Rb- and Cs-ZK-5 zeolites. *RSC Advances* **2014**, 4, (107), 62511-62524.
- 458 4. Ryckebosch, E.; Drouillon, M.; Vervaeren, H., Techniques for transformation of biogas  
459 to biomethane. *Biomass and Bioenergy* **2011**, 35, (5), 1633-1645.
- 460 5. Delgado, J. A.; Uguina, M. A.; Sotelo, J. L.; Ruíz, B.; Rosário, M., Carbon  
461 Dioxide/Methane Separation by Adsorption on Sepiolite. *Journal of Natural Gas Chemistry*  
462 **2007**, 16, (3), 235-243.
- 463 6. Petersson, A.; Wellinger, A. *Biogas upgrading technologies-developments and*  
464 *innovations*; Task 37 - Energy from biogas and landfill gas: 2009.
- 465 7. Sarkar, S. C.; Bose, A., Role of activated carbon pellets in carbon dioxide removal.  
466 *Energy Conversion and Management* **1997**, 38, Supplement, S105-S110.
- 467 8. Horikawa, M. S.; Rossi, F.; Gimenes, M. L.; Costa, C. M. M.; Da Silva, M. G. C.,  
468 Chemical absorption of H<sub>2</sub>S for biogas purification. *Brazilian Journal of Chemical Engineering*  
469 **2004**, 21, (3), 415-422.
- 470 9. Yeo, Z. Y.; Chew, T. L.; Zhu, P. W.; Mohamed, A. R.; Chai, S.-P., Conventional  
471 processes and membrane technology for carbon dioxide removal from natural gas: A review.  
472 *Journal of Natural Gas Chemistry* **2012**, 21, (3), 282-298.
- 473 10. Tuinier, M. J.; van Sint Annaland, M., Biogas Purification Using Cryogenic Packed-Bed  
474 Technology. *Industrial & Engineering Chemistry Research* **2012**, 51, (15), 5552-5558.
- 475 11. Grande, C. A., Biogas Upgrading by Pressure Swing Adsorption In *Biofuel's Engineering*  
476 *Process Technology*, Bernardes, M. A. D. S., Ed. InTech: 2011; pp 65-84.
- 477 12. Kim, S.; Kim, J.; Moon, I., Profit optimization for bio-gas upgrading PSA process based  
478 on controlling step-time. In *Computer Aided Chemical Engineering*, 2013; Vol. 32, pp 397-402.
- 479 13. Grande, C. A.; Rodrigues, A. E., Layered vacuum pressure-swing adsorption for biogas  
480 upgrading. *Industrial and Engineering Chemistry Research* **2007**, 46, (23), 7844-7848.
- 481 14. Peter, S. A.; Baron, G. V.; Gascon, J.; Kapteijn, F.; Denayer, J. F. M., Dynamic  
482 desorption of CO<sub>2</sub> and CH<sub>4</sub> from amino-MIL-53(Al) adsorbent. *Adsorption* **2013**, 19, (6), 1235-  
483 1244.
- 484 15. Sircar, S., Separation of Methane and Carbon Dioxide Gas Mixtures by Pressure Swing  
485 Adsorption. *Separation Science and Technology* **1988**, 23, (6-7), 519-529.
- 486 16. Kim, M.-B.; Bae, Y.-S.; Choi, D.-K.; Lee, C.-H., Kinetic Separation of Landfill Gas by a  
487 Two-Bed Pressure Swing Adsorption Process Packed with Carbon Molecular Sieve:  
488 Nonisothermal Operation. *Industrial & Engineering Chemistry Research* **2006**, 45, (14), 5050-  
489 5058.

17. Yanh, R. T., *Adsorbents. Funtamentals and applications.* . John Wiley & Sons: New Jersey, 2003.
18. Cavenati, S.; Grande, C. A.; Rodrigues, A. E., Removal of carbon dioxide from natural gas by vacuum pressure swing adsorption. *Energy & Fuels* **2006**, 20, (6), 2648-2659.
19. Kapoor, A.; Yang, R. T., Kinetic separation of methane-carbon dioxide mixture by adsorption on molecular sieve carbon. *Chemical Engineering Science* **1989**, 44, (8), 1723-1733.
20. Alonso-Vicario, A.; Ochoa-Gómez, J. R.; Gil-Río, S.; Gómez-Jiménez-Aberasturi, O.; Ramírez-López, C. A.; Torrecilla-Soria, J.; Domínguez, A., Purification and upgrading of biogas by pressure swing adsorption on synthetic and natural zeolites. *Microporous and Mesoporous Materials* **2010**, 134, (1-3), 100-107.
21. Cavenati, S.; Grande, C. A.; Rodrigues, A. E., Upgrade of Methane from Landfill Gas by Pressure Swing Adsorption. *Energy & Fuels* **2005**, 19, (6), 2545-2555.
22. Cavenati, S.; Grande, C. A.; Rodrigues, A. E., Adsorption Equilibrium of Methane, Carbon Dioxide, and Nitrogen on Zeolite 13X at High Pressures. *Journal of Chemical and Engineering Data* **2004**, 49, (4), 1095-1101.
23. Leyssale, J. M.; Papadopoulos, G. K.; Theodorou, D. N., Sorption thermodynamics of CO<sub>2</sub>, CH<sub>4</sub>, and their mixtures in the ITQ-1 zeolite as revealed by molecular simulations. *Journal of Physical Chemistry B* **2006**, 110, (45), 22742-22753.
24. Babarao, R.; Hu, Z.; Jiang, J.; Chempath, S.; Sandler, S. I., Storage and separation of CO<sub>2</sub> and CH<sub>4</sub> in silicalite, C168 schwarzite, and IRMOF-1: A comparative study from Monte Carlo simulation. *Langmuir* **2007**, 23, (2), 659-666.
25. Bae, Y.-S.; Mulfort, K. L.; Frost, H.; Ryan, P.; Punnnathanam, S.; Broadbelt, L. J.; Hupp, J. T.; Snurr, R. Q., Separation of CO<sub>2</sub> from CH<sub>4</sub> Using Mixed-Ligand Metal–Organic Frameworks. *Langmuir* **2008**, 24, (16), 8592-8598.
26. Barcia, P. S.; Bastin, L.; Hurtado, E. J.; Silva, J. A. C.; Rodrigues, A. E.; Chen, B., Single and multicomponent sorption of CO<sub>2</sub>, CH<sub>4</sub> and N<sub>2</sub> in a microporous metal-organic framework. *Separation Science and Technology* **2008**, 43, (13), 3494-3521.
27. Liang, Z.; Marshall, M.; Chaffee, A. L., CO<sub>2</sub> Adsorption-Based Separation by Metal Organic Framework (Cu-BTC) versus Zeolite (13X). *Energy & Fuels* **2009**, 23, (5), 2785-2789.
28. Peng, X.; Wang, W. C.; Xue, R. S.; Shen, Z. M., Adsorption separation of CH<sub>4</sub>/CO<sub>2</sub> on mesocarbon microbeads: Experiment and modeling. *AIChE Journal* **2006**, 52, (3), 994-1003.
29. Goetz, V.; Pupier, O.; Guillot, A., Carbon dioxide-methane mixture adsorption on activated carbon. *Adsorption* **2006**, 12, (1), 55-63.
30. Bazan, R. E.; Bastos-Neto, M.; Staudt, R.; Papp, H.; Azevedo, D. C. S.; Cavalcante Jr, C. L., Adsorption equilibria of natural gas components on activated carbon: Pure and mixed gas isotherms. *Adsorption Science and Technology* **2008**, 26, (5), 323-332.
31. Santos, M. P. S.; Grande, C. A.; Rodrigues, A. E., Dynamic study of the pressure swing adsorption process for biogas upgrading and its responses to feed disturbances. *Industrial & Engineering Chemistry Research* **2013**, 52, (15), 5445-5454.
32. Son, S.-J.; Choi, J.-S.; Choo, K.-Y.; Song, S.-D.; Vijayalakshmi, S.; Kim, T.-H., Development of carbon dioxide adsorbents using carbon materials prepared from coconut shell. *Korean Journal of Chemical Engineering* **2002**, 19, (2), 291-297.
33. Sun, Y.; Webley, P. A., Preparation of activated carbons with large specific surface areas from biomass corncob and their adsorption equilibrium for methane, carbon dioxide, nitrogen, and hydrogen. *Industrial & Engineering Chemistry Research* **2011**, 50, (15), 9286-9294.

34. Banisheykholeslami, F.; Ghoreyshi, A. A.; Mohammadi, M.; Pirzadeh, K., Synthesis of a carbon molecular sieve from broom corn stalk via carbon deposition of methane for the selective separation of a CO<sub>2</sub>/CH<sub>4</sub> mixture. *Clean - Soil, Air, Water* **2015**, 43, (7), 1084-1092.
35. Álvarez-Gutiérrez, N.; Gil, M. V.; Rubiera, F.; Pevida, C., Adsorption performance indicators for the CO<sub>2</sub>/CH<sub>4</sub> separation: Application to biomass-based activated carbons. *Fuel Processing Technology* **2016**, 142, 361-369.
36. Álvarez-Gutiérrez, N.; Gil, M. V.; Rubiera, F.; Pevida, C., Cherry-stones-based activated carbons as potential adsorbents for CO<sub>2</sub>/CH<sub>4</sub> separation: effect of the activation parameters. *Greenhouse Gases: Science and Technology* **2015**, 5, (6), 812-825.
37. Gil, M. V.; Álvarez-Gutiérrez, N.; Martínez, M.; Rubiera, F.; Pevida, C.; Morán, A., Carbon adsorbents for CO<sub>2</sub> capture from bio-hydrogen and biogas streams: Breakthrough adsorption study. *Chemical Engineering Journal* **2015**, 269, 148-158.
38. García, S.; Pis, J. J.; Rubiera, F.; Pevida, C., Predicting mixed-gas adsorption equilibria on activated carbon for precombustion CO<sub>2</sub> capture. *Langmuir* **2013**, 29, (20), 6042-6052.
39. García, S.; Gil, M. V.; Martín, C. F.; Pis, J. J.; Rubiera, F.; Pevida, C., Breakthrough adsorption study of a commercial activated carbon for pre-combustion CO<sub>2</sub> capture. *Chemical Engineering Journal* **2011**, 171, (2), 549-556.
40. Ruthven, D. M.; Farooq, S.; Knaebel, K. S., *Pressure Swing Adsorption*. VCH Publishers: New York, 1994.
41. Finsy, V.; Ma, L.; Alaerts, L.; De Vos, D. E.; Baron, G. V.; Denayer, J. F. M., Separation of CO<sub>2</sub>/CH<sub>4</sub> mixtures with the MIL-53(Al) metal-organic framework. *Microporous and Mesoporous Materials* **2009**, 120, (3), 221-227.
42. Pirngruber, G. D.; Hamon, L.; Bourrelly, S.; Llewellyn, P. L.; Lenoir, E.; Guillermin, V.; Serre, C.; Devic, T., A method for screening the potential of MOFs as CO<sub>2</sub> adsorbents in pressure swing adsorption processes. *ChemSusChem* **2012**, 5, (4), 762-776.
43. McCabe, W. L.; Smith, J. C.; Harriott, P., *Unit operations of chemical engineering*. Seventh ed.; Mc Graw-Hill: 2005.
44. Martín, C. F.; García, S.; Beneroso, D.; Pis, J. J.; Rubiera, F.; Pevida, C., Precombustion CO<sub>2</sub> capture by means of phenol-formaldehyde resin-derived carbons: From equilibrium to dynamic conditions. *Separation and Purification Technology* **2012**, 98, 531-538.
45. Martín, C. F.; Stöckel, E.; Clowes, R.; Adams, D. J.; Cooper, A. I.; Pis, J. J.; Rubiera, F.; Pevida, C., Hypercrosslinked organic polymer networks as potential adsorbents for pre-combustion CO<sub>2</sub> capture. *Journal of Materials Chemistry* **2011**, 21, (14), 5475-5483.
46. Martín, C. F.; Plaza, M. G.; Pis, J. J.; Rubiera, F.; Pevida, C.; Centeno, T. A., On the limits of CO<sub>2</sub> capture capacity of carbons. *Separation and Purification Technology* **2010**, 74, (2), 225-229.
47. Wiersum, A. D.; Giovannangeli, C.; Vincent, D.; Bloch, E.; Reinsch, H.; Stock, N.; Lee, J. S.; Chang, J. S.; Llewellyn, P. L., Experimental screening of porous materials for high pressure gas adsorption and evaluation in gas separations: Application to MOFs (MIL-100 and CAU-10). *ACS Combinatorial Science* **2013**, 15, (2), 111-119.
48. Yu, H.; Wang, X.; Xu, C.; Chen, D. L.; Zhu, W.; Krishna, R., Utilizing transient breakthroughs for evaluating the potential of Kureha carbon for CO<sub>2</sub> capture. *Chemical Engineering Journal* **2015**, 269, 135-147.
49. Kumar, R., Pressure Swing Adsorption Process: Performance Optimum and Adsorbent Selection. *Industrial & Engineering Chemistry Research* **1994**, 33, (6), 1600-1605.



50. Krishna, R., Adsorptive separation of CO<sub>2</sub>/CH<sub>4</sub>/CO gas mixtures at high pressures. *Microporous and Mesoporous Materials* **2012**, 156, (0), 217-223.
51. Wu, H.; Yao, K.; Zhu, Y.; Li, B.; Shi, Z.; Krishna, R.; Li, J., Cu-TDPAT, an rht-type dual-functional metal–organic framework Offering significant potential for use in H<sub>2</sub> and natural gas purification processes operating at high pressures. *The Journal of Physical Chemistry C* **2012**, 116, (31), 16609-16618.

611 **Table 1.** Physical properties of the activated carbons

	Activated carbon		
	CS-CO <sub>2</sub>	CS-H <sub>2</sub> O	Calgon BPL
BET surface area (m <sup>2</sup> g <sup>-1</sup> )	1045	998	1129
Total pore volume (cm <sup>3</sup> g <sup>-1</sup> )	0.48	0.53	0.50
Micropore volume (cm <sup>3</sup> g <sup>-1</sup> ) <sup>a</sup>	0.40	0.38	0.46
Average micropore width (nm) <sup>b</sup>	0.93	0.89	1.40
Narrow Micropore volume (cm <sup>3</sup> g <sup>-1</sup> ) <sup>a</sup>	0.35	0.33	0.22
Average narrow micropore width (nm) <sup>b</sup>	0.78	0.74	0.70

612 <sup>a</sup> Evaluated with the Dubinin-Radushkevich equation.613 <sup>b</sup> Determined with the Stoeckli-Ballerini relation.

614

615

616

617 **Table 2.** Characteristics of the adsorbent beds

	Activated carbon		
	CS-CO <sub>2</sub>	CS-H <sub>2</sub> O	Calgon BPL
Mass of adsorbent (g)	4.10	4.80	7.00
Particle size (mm)	1-3	1-3	2-4.75
Total porosity, $\epsilon_T$	0.86	0.84	0.79
Helium density (g cm <sup>-3</sup> ) <sup>a</sup>	1.98	1.99	2.10
Apparent density (g cm <sup>-3</sup> ) <sup>b</sup>	0.53	0.64	0.83
Bed diameter (cm)	1.30	1.30	1.30
Bed height (cm)	11.55	11.65	11.90
Bed density (g cm <sup>-3</sup> )	0.27	0.31	0.44

618 <sup>a</sup> Determined by He pycnometry.619 <sup>b</sup> Determined with Hg porosimetry at 1 bar.

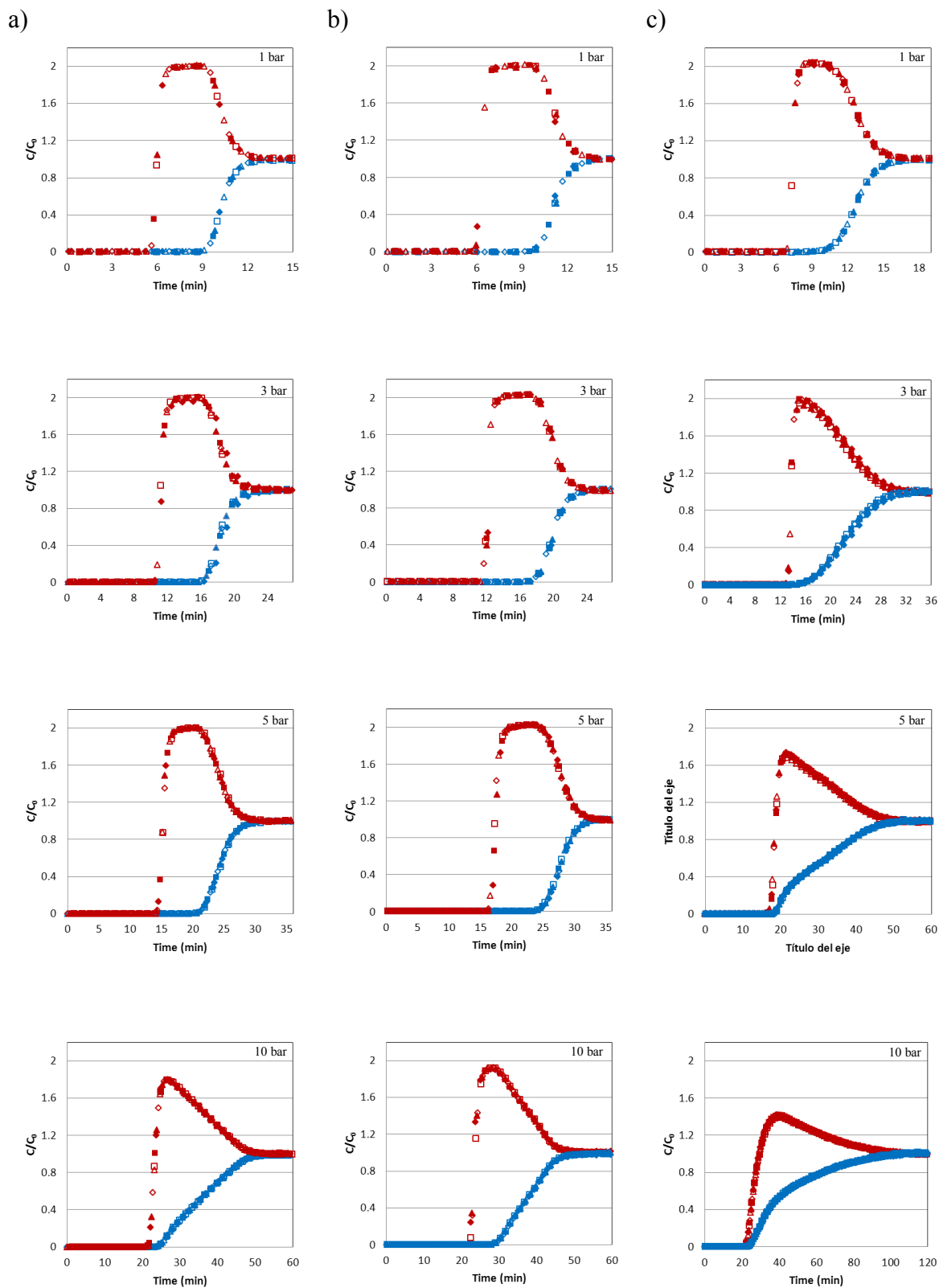
620

621

622

**Table 3.** Adsorbed amounts for breakthrough measurements of a simulated biogas CO<sub>2</sub>/CH<sub>4</sub> mixture (50/50 vol. %) at 30 °C and different pressures on CS-CO<sub>2</sub>, CS-H<sub>2</sub>O, and Calgon BPL.

Adsorbent	CO <sub>2</sub> adsorption capacity		CH <sub>4</sub> adsorption capacity	
	(mol kg <sup>-1</sup> )	(mol m <sup>-3</sup> )	(mol kg <sup>-1</sup> )	(mol m <sup>-3</sup> )
1 bar				
CS-CO <sub>2</sub>	1.63	440.1	0.47	126.9
CS-H <sub>2</sub> O	1.49	461.9	0.37	114.7
Calgon BPL	1.18	519.2	0.33	145.2
3 bar				
CS-CO <sub>2</sub>	2.80	756.0	0.67	180.9
CS-H <sub>2</sub> O	2.60	806.0	0.64	198.4
Calgon BPL	2.02	888.8	0.53	233.2
5 bar				
CS-CO <sub>2</sub>	3.60	972.0	0.95	256.5
CS-H <sub>2</sub> O	3.53	1094.3	0.76	235.6
Calgon BPL	2.70	1188.0	0.81	356.4
10 bar				
CS-CO <sub>2</sub>	5.14	1387.8	1.55	418.5
CS-H <sub>2</sub> O	4.48	1388.8	1.05	325.5
Calgon BPL	4.14	1821.6	1.30	572.0

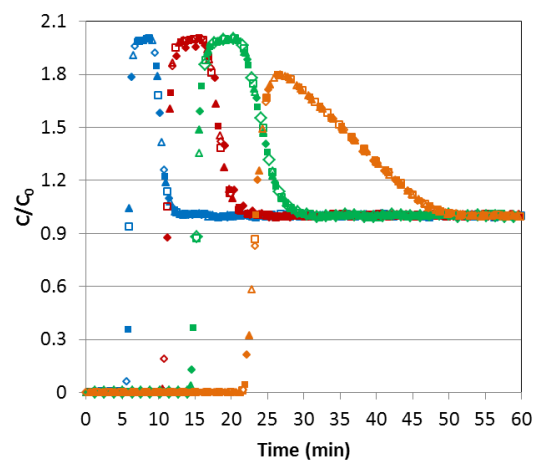
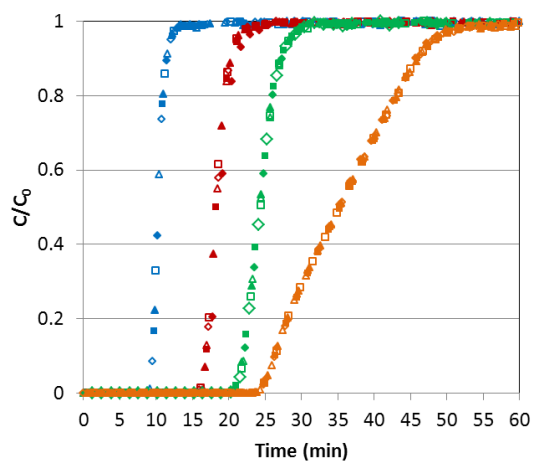


632

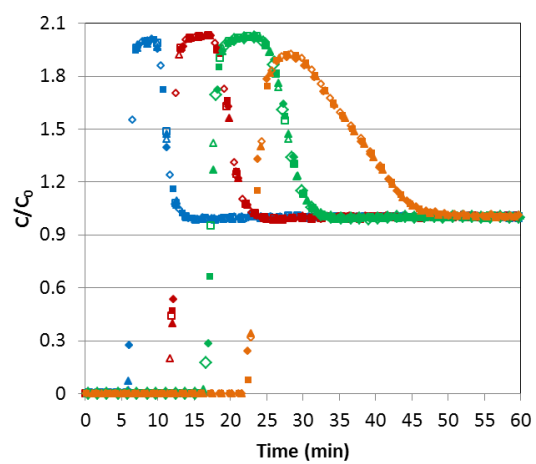
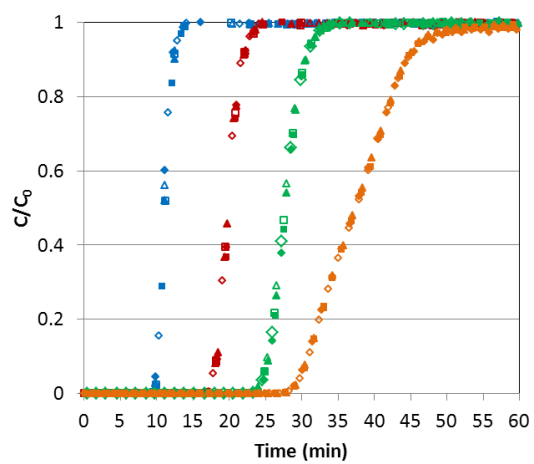
633 **Figure 1.** CO<sub>2</sub> (blue) and CH<sub>4</sub> (red) breakthrough curves of the experiments with CO<sub>2</sub>/CH<sub>4</sub>  
634 mixture (50/50 vol. %) in feed gas for CS-CO<sub>2</sub> (a), CS-H<sub>2</sub>O (b), and Calgon BPL (c) at 1, 3, 5,  
635 and 10 bar and at 30 °C. The six consecutive cycles are represented by the different symbols: ♦  
636 cycle 1, ▲ cycle 2, ■ cycle 3, ◇ cycle 4, △ cycle 5, □ cycle 6.

637

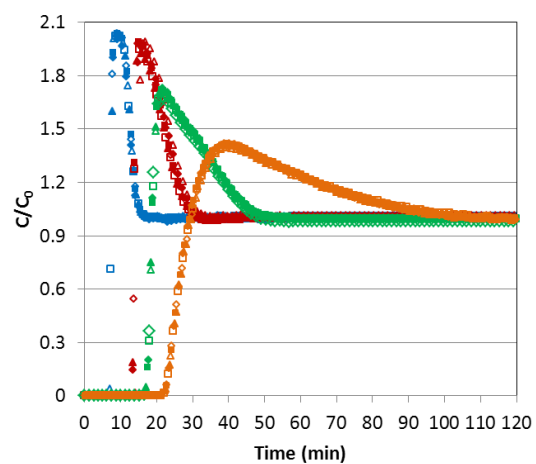
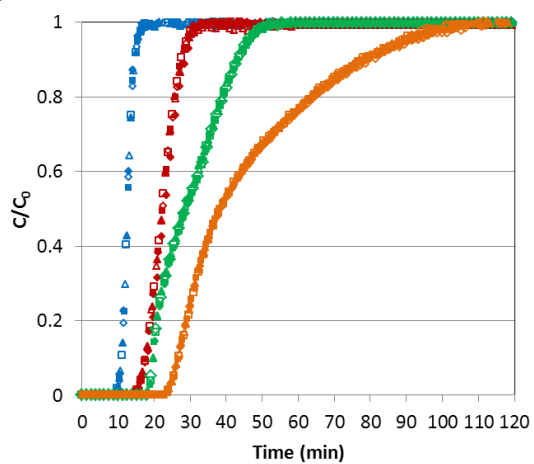
a)



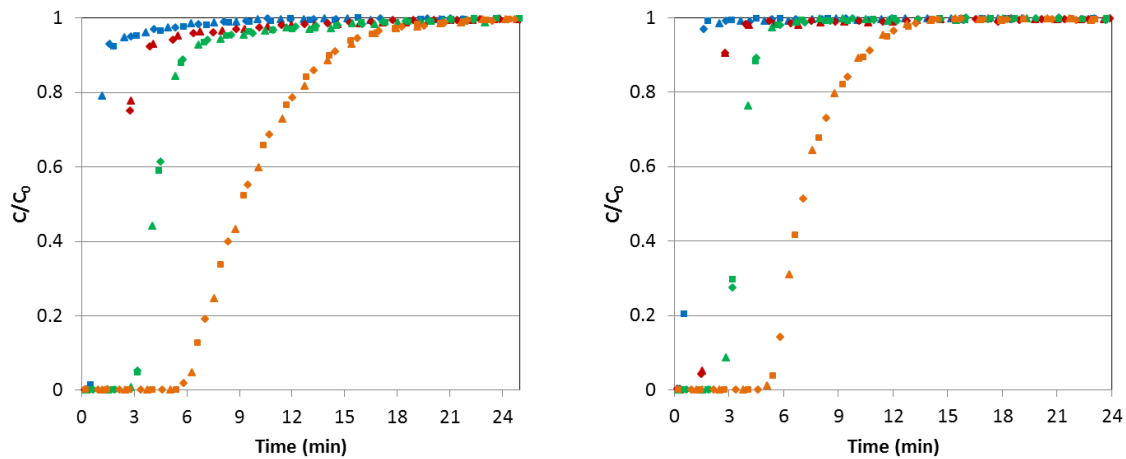
b)



c)



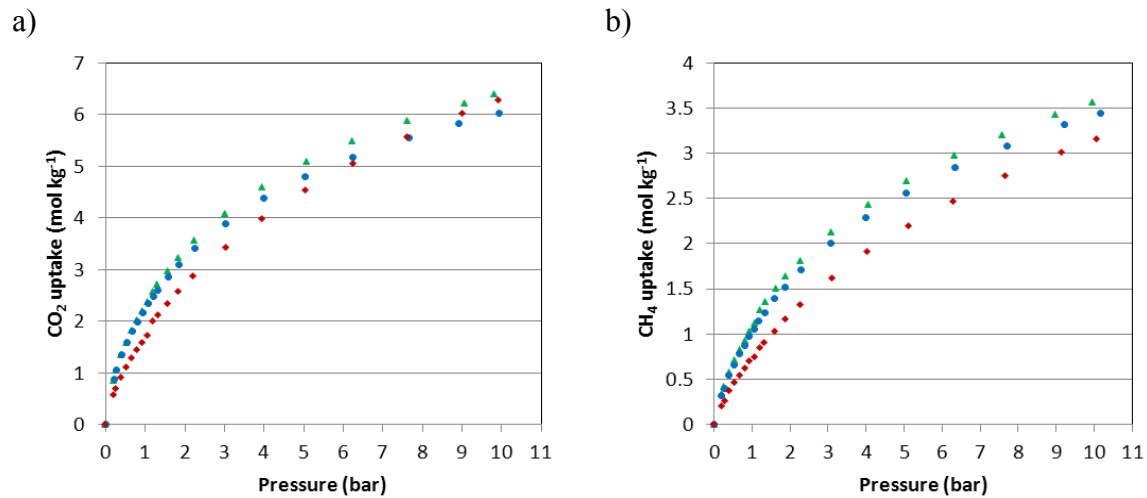
d)



638 **Figure 2.** Comparison of CO<sub>2</sub> (left graphs) and CH<sub>4</sub> (right graphs) breakthrough curves at the  
639 evaluated pressures for CS-CO<sub>2</sub> (a), CS-H<sub>2</sub>O (b), Calgon BPL (c) and Blank experiments (d). 1  
640 bar (blue), 3 bar (red), 5 bar (green), 10 bar (orange). Feed: CO<sub>2</sub>/CH<sub>4</sub> mixture (50/50 vol. %) at  
641 30 °C.

642

643

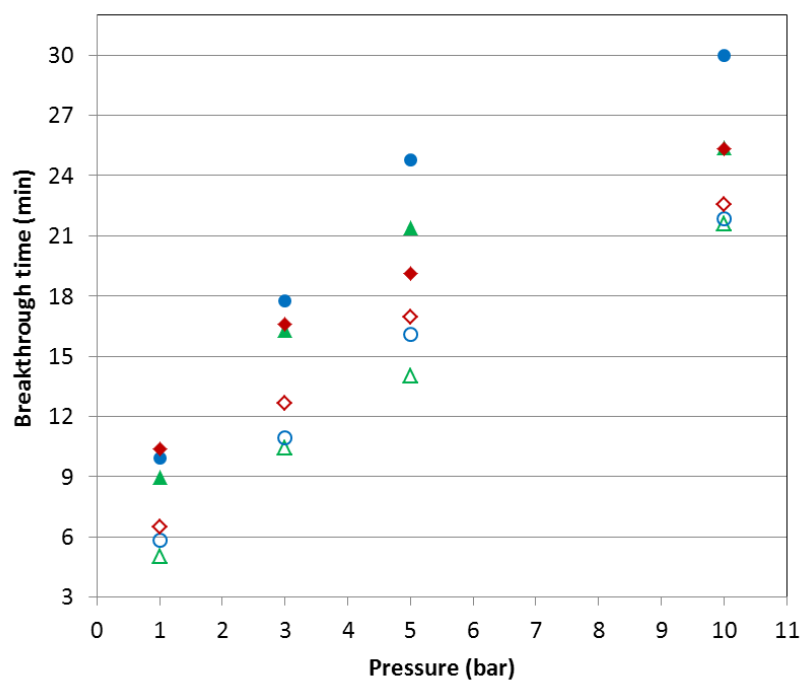


644 **Figure 3.** Adsorption isotherms at 30 °C and up to 10 bar of CO<sub>2</sub> (a) and CH<sub>4</sub> (b) on CS-CO<sub>2</sub>  
 645 (green colour), CS-H<sub>2</sub>O (blue colour), and Calgon-BPL (red colour).

646



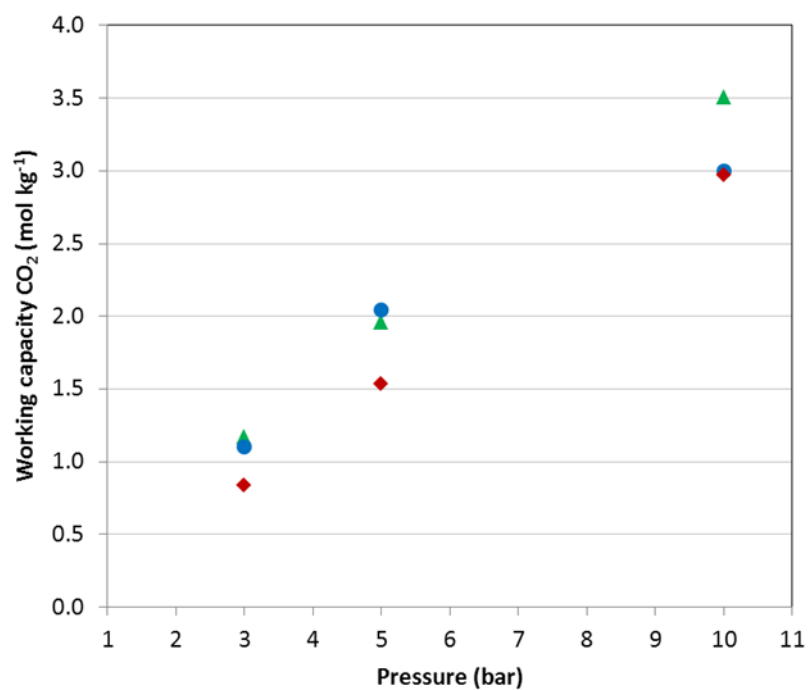
647



648 **Figure 4.** CO<sub>2</sub> (full symbols) and CH<sub>4</sub> (open symbols) breakthrough times as a function of  
649 pressure: CS-CO<sub>2</sub> (green colour), CS-H<sub>2</sub>O (blue colour), and Calgon BPL (red colour). Feed:  
650 CO<sub>2</sub>/CH<sub>4</sub> mixture (50/50 vol. %) at 30 °C.  
651

652

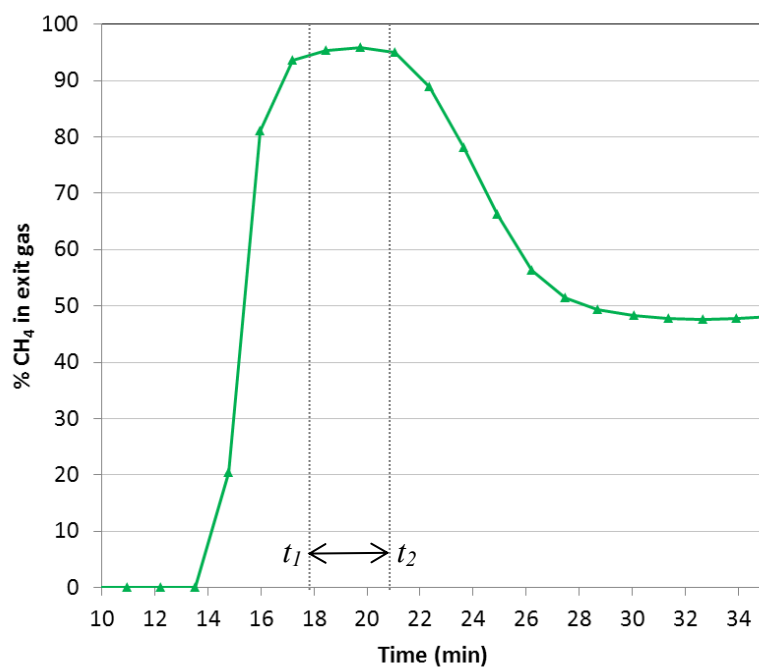
653



654 **Figure 5.** Working capacity of CO<sub>2</sub> as a function of pressure for CS-CO<sub>2</sub> (green colour), CS-  
 655 H<sub>2</sub>O (blue colour), and Calgon BPL (red colour). Values estimated from binary breakthrough  
 656 tests.

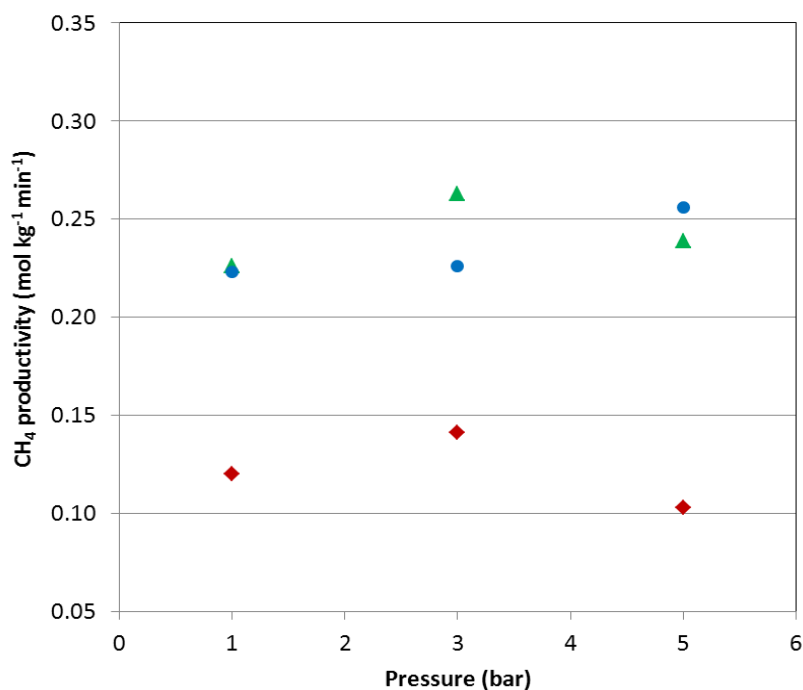
657

658



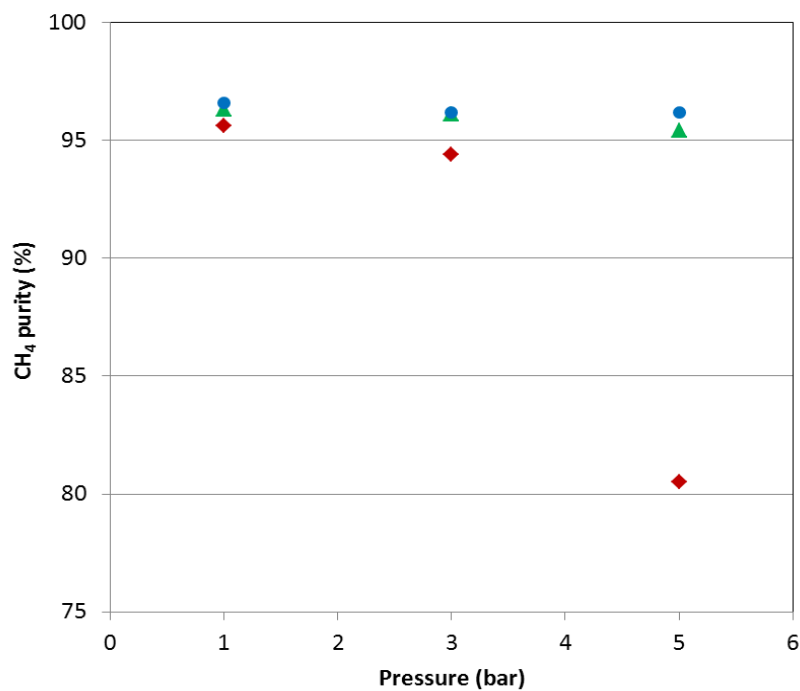
659 **Figure 6.** CH<sub>4</sub> breakthrough for CO<sub>2</sub>/CH<sub>4</sub> mixture (50/50 vol. %) at 30 °C and at 5 bar in the  
 660 fixed bed packed with CS-CO<sub>2</sub>.

661



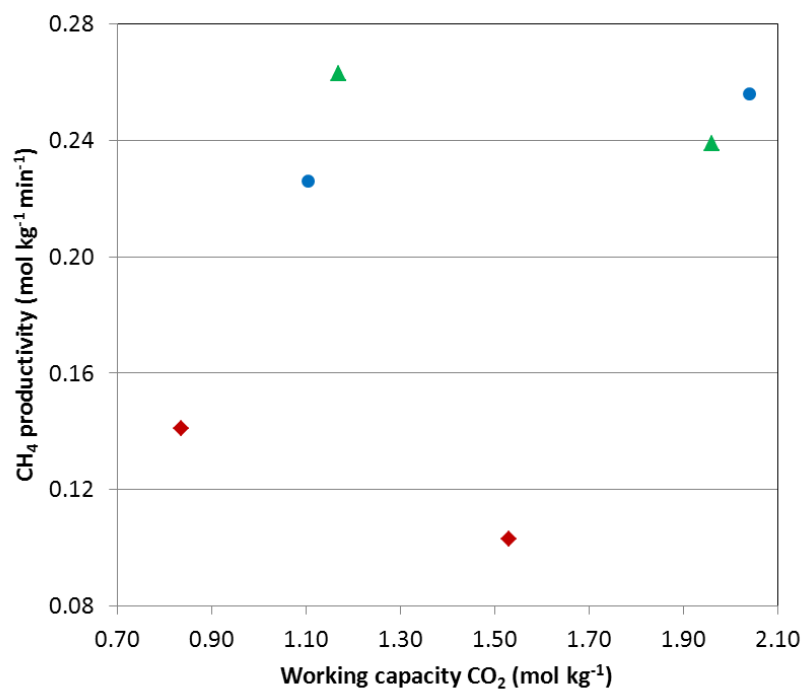
663 **Figure 7.** CH<sub>4</sub> productivity versus pressure for CS-CO<sub>2</sub> (green symbols), CS-H<sub>2</sub>O (blue  
 664 symbols), and Calgon BPL (red symbols). Values estimated from binary breakthrough tests  
 665 (section 3.1). Note:  $t_1$  and  $t_2$  were selected for each adsorbent at each pressure according to the  
 666 criteria of maximum CH<sub>4</sub> purity in the outlet gas stream.

667



669 **Figure 8.** Purity of CH<sub>4</sub> in the outlet gas stream as a function of pressure for CS-CO<sub>2</sub> (green  
 670 symbols), CS-H<sub>2</sub>O (blue symbols), and Calgon BPL (red symbols). Values estimated from  
 671 binary breakthrough tests.  
 672

674



675 **Figure 9.** Productivity of CH<sub>4</sub> versus the CO<sub>2</sub> working capacity for CS-CO<sub>2</sub> (green symbols),  
 676 CS-H<sub>2</sub>O (blue symbols), and Calgon BPL (red symbols). Values estimated from binary  
 677 breakthrough tests.  
 678

679

680

681

682